ISBN: 978-3-95450-191-5 doi:10.18429/JACoW-SRF2017-MOPB090

SUB-MICRO-TESLA MAGNETIC SHIELDING DESIGN FOR CRYOMODULES IN THE HIGH-GRADIENT PROGRAM AT CERN

S. Papadopoulos*, L. Dassa, J. P. Dequaire, F. Gerigk,
F. Pillon, S. Ramberger, P. Yilmazer
CERN, Geneva, Switzerland

Abstract

In the framework of the High-Gradient R&D program at CERN a cryomodule, consisting of four superconducting 5-cell cavities, has been designed. In order to reduce flux trapping in the surface of the superconductor and to minimize Q degradation during a quench, highly effective magnetic shielding is needed. The solution proposed includes cold and warm passive shielding enhanced by four compensating coils. In this paper the magneto-static simulation results are presented illustrating different design considerations that led to a final design. Finally the shielding ability of the vacuum vessel is investigated experimentally through ambient magnetic field measurements.

INTRODUCTION

The High-Gradient (HG) test cryomodule contains four 5-cell bulk Nb $RRR = 300$ superconducting cavities operating at 704.4 MHz. The design Q-factor of 10^{10} will allow an operation with 25 MV/m accelerating gradient. For reaching this value the average surface resistance needs to be $R_s \leq 27\,\mathrm{n\Omega}$.

Trapped Flux Surface Resistance

The overall surface resistance R_s is given by the sum of the different loss mechanisms (Eq. (1)):

$$R_s = R_{BCS} + R_{TF} + R_{res} \tag{1}$$

where R_{BCS} is the BCS surface resistance, R_{TF} is the resistance due to trapped magnetic flux and R_{res} is any other residual resistance due to impurities and lattice disruptions. For the HG cavities $R_{BCS} = 6\,\mathrm{n\Omega}$ [1] and the expected $R_{res} = 10\,\mathrm{n\Omega}$. These values allow an $R_{TF} \leq 11\,\mathrm{n\Omega}$. With a trapped-flux sensitivity of around 2.2 nΩ/μT [2] the maximum ambient magnetic field on the cavity surface needs to be $B_{amb} \leq 5\,\mu\mathrm{T}$.

Nevertheless, recent studies [3] illustrate the strong relation between trapped magnetic flux and quenching while full recovery of the Q-factor after quenching is possible only in absence of ambient magnetic field. This motivates the investigation and design of a sub-μT magnetic shielding solution that will ensure stability and high-performance during operation.

Magnetic Shielding Factor

The *magnetic shielding factor S* of a magnetic shield is defined as the ratio of the external magnetic field over the magnetic field at the center of the shield: $S = B_{ext}/B_{center}$. Analytical expressions exist for the calculation of the shielding factor for the simple case of a cylindrical shield. The shielding factor of a magnetic shield depends on the orientation of the magnetic field. The parallel shielding factor $S_\parallel$ refers to the case of a magnetic field parallel to the central axis of the shield. The perpendicular shielding factor $S_\perp$ refers to the case of a magnetic field perpendicular to the central axis of the shield. The $S_\parallel$ is different for cylinders with open and closed ends. The relevant formulas are given in Eqs. (2), (3), and (4).

$$S_\perp = \frac{\mu \cdot d}{D}, \tag{2}$$

$$S_\parallel^{open} = 4NS_\perp + 1 \tag{3}$$

$$S_\parallel^{closed} = \frac{S_\parallel^{open}}{1 + D/2L} \tag{4}$$

where μ is the magnetic permeability of the material, d is the thickness of the shield, D is the diameter of the cylinder, L is the length and N is the demagnetization factor [4]. The demagnitization factor N is a function of the ratio L/D. Measurements and calculations concerning the demagnetization factor of cylinders can be found in [5–7]. The equations assume linear magnetic material and give a good idea for the initial parameters of the needed shield. Nevertheless, the impact of saturation due to material non-linearities, the high complexity of the shield to fit the mechanical design of the cryomodule and the need for extensive shielding optimisation, not only at the center of the shield but in the whole area of the cavity surface require detailed magnetostatic simulations.

MAGNETIC SHIELDING DESIGN

Magnetic Shielding Materials

The design proposed includes a warm magnetic shield close to the interior side of the vacuum vessel and four cold shields around the helium vessel of the cavities. For the manufacturing of the cold shield cryophy® material has been chosen as it is specifically developed for reaching a high relative magnetic permeability value at cryogenic temperatures [8]. The highly permeable mu-metal material can be used for the warm shield. For the magneto-static simulations, manufacturers of mu-metal and cryophy® suggest the use of the following values: $\mu_r^{mumetal} = 50000$ and $\mu_r^{cryophy} = 15000$ [9, 10]. The shielding system is shown in Figure 1.

* sotirios.papadopoulos@cern.ch

ISBN: 978-3-95450-191-5 doi:10.18429/JACoW-SRF2017-MOPB090

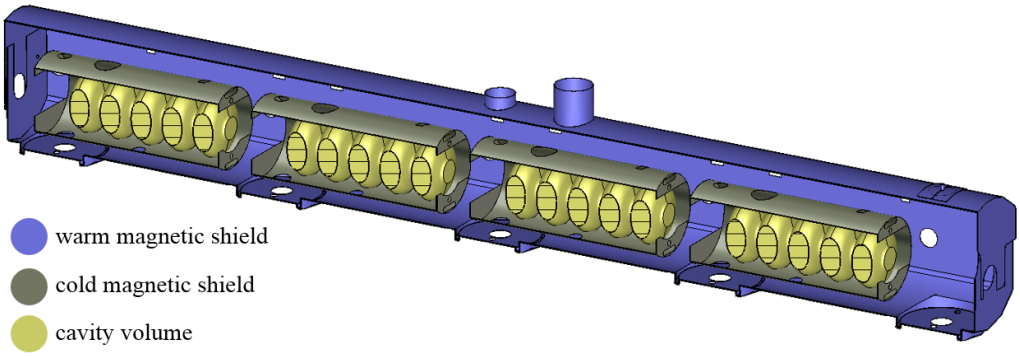

Figure 1: Sliced view of the HG test cryomodule passive magnetic shielding design.

Theoretical Treatment of the Shielding Design

The earth's magnetic field is around 50 μT [11]. A shielding factor of $S = 500$ is needed in order to reach 0.1 μT magnetic field on the cavities. The orientation of the shield relative to the external magnetic field is not yet defined, thus the design assumes a magnetic field of 50 μT in both directions, perpendicular and parallel with respect to the shield. Since $N \ll 0.25$ for structures with $L/D < 2$, Equation (3) shows that the parallel field is in general more difficult to shield in comparison with the perpendicular. Thus, it is justified to focus on optimising the $S_{\parallel}$. For the beginning we assume perfect cylindrical shields with open ends. A cold cryophy® magnetic shield can be placed around the helium vessel of the cavity with $L = 1600$ mm and $D = 500$ mm. The thickness of the shield is restricted to $d = 1$ mm for mechanical integration reasons. In this case is $S_{\parallel cold}^{open} = 21$. By nesting the two shields and with a distance between them ensuring magnetic de-coupling we can increase significantly the total shielding factor ($S_{\parallel total}$). More specifically, the $S_{\parallel total}$ will be the product of the two individual shielding factors (Eq. (5)).

$$S_{\parallel total} = S_{\parallel\, warm}^{\,open} \cdot S_{\parallel\, cold}^{\,open} \tag{5}$$

For reaching $S_{\parallel total} = 500$ the $S_{\parallel warm}^{open}$ should be > 24. Taking also into account the dimensions of the vacuum vessel for a length $L = 6600$ mm and a diameter $D = 700$ mm we conclude to a thickness $d = 2$ mm for the warm mu-metal shield. It is important to note that the calculation of $S_{\parallel total}$ assumes perfect cylinders and magnetically decoupled shields. However, in reality the shields are not perfect cylinders and they accommodate many holes and openings. In addition, the shields are not perfectly de-coupled leading to a decrease of the shielding factor. Moreover, the $S_{\parallel total}$ calculated gives the shielding efficiency for the center of the shielding system, while our design needs an $S > 500$ all over the surface of the cavity. Finally, a shield with high L/D, as the warm shield in our case, concentrates very high magnetic fields inside its material. For a thinner material the field is higher and saturation effects might have an impact on the shielding efficiency. For these reasons the thickness d of the warm magnetic shielding is chosen to be 3 mm giving a theoretical $S_{\parallel total} = 840$. A more detailed design has been realised with the use of magnetostatic simulations.

MAGNETOSTATIC SIMULATION RESULTS

The simulation results that follow were realised with the CST EM Studio®.

Cold Magnetic Shield

The cold magnetic shield is situated just outside the helium vessel. Because of mechanical restrictions concerning the position of the tuner on the side of the cavity the shield presents a big hole on this side (Fig. 2).

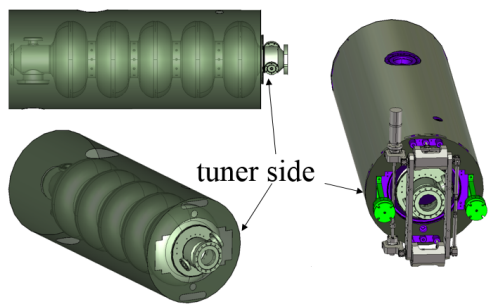

Figure 2: Cold magnetic shield design. The tuner situated on the side of the cavity requires positioning the cavity close to the end of the shield.

Since the tuner is attached on the cavity, the cavity is very close to the hole. Figure 3 shows the absolute value of the magnetic field on the cavity surface in the case of the cold shield for an applied field $B = 50$ μT perpendicular ($B_{\perp}$) and parallel ($B_{\parallel}$) to the beam axis. In the case of $B_{\parallel}$ the $S_{\parallel}$ drops significantly for a big part of the cell near the tuner (Fig. 4). In the case of $B_{\perp}$ the tuner hole introduces only a small $S_{\perp}$ deterioration in a low surface current region of the cavity. The hole at the top of the shield, has also an impact on the $S_{\perp}$ as it can be seen in Fig. 4 between 200 mm and 500 mm. This hole serves as a passage for the cryogenic supply to the helium vessel and its diameter cannot be reduced.

ISBN: 978-3-95450-191-5 doi:10.18429/JACoW-SRF2017-MOPB090

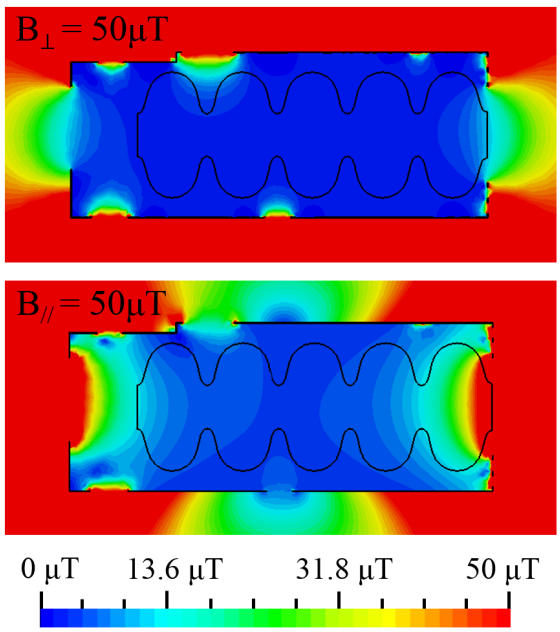

Figure 3: Cold magnetic shield simulation. Absolute value of the magnetic field for the cases of $B_\perp$ (up) and $B_\parallel$ (down).

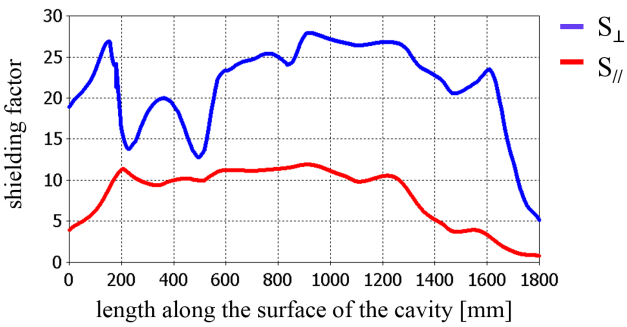

Figure 4: Rotationally averaged shielding factor along the surface of the cavity for both directions of the applied field.

Combination of Warm and Cold Magnetic Shield

For further enhancing the shielding efficiency a warm magnetic shield has been designed to be situated near the inner surface of the vacuum vessel covering the four cold shields around the cavities (Fig. 1). The simulation results combining the two shields prove an important increase of the shielding factor. Figure 5 shows the absolute value of the magnetic field in the case of the combination of the cold and warm shields for a magnetic field of $B = 50\,\mu T$ perpendicular ($B_\perp$) and parallel ($B_\parallel$) to the beam axis. It can be seen that the $S_\perp$ has reached values from 400 to 3000. $B_\perp$ is very effectively shielded. The most important source of penetrating field is located at the bottom of the shield through the holes designed to accommodate the power coupler. Penetration from the holes at the top of the warm shield was avoided by placing shielding tubes around them. In the case of $B_\parallel$ the penetration from the hole at the top of the cold shield has now been reduced. However, the penetrating

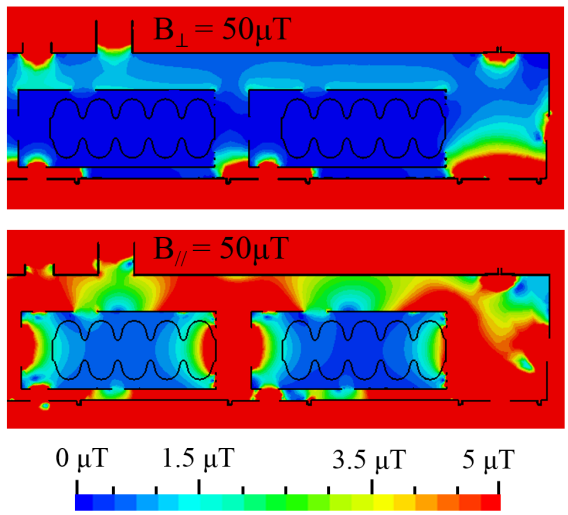

Figure 5: Cold and warm magnetic shield simulation. Absolute value of the magnetic field for the case of $B_\perp$ (up) and $B_\parallel$ (down). Only half shield is presented.

field from the tuner side still reduces the shielding factor in this area to values lower than 10. The warm shield increased the $S_\parallel$ by a factor of 10 however the $S_\parallel$ =500 threshold value was not reached.

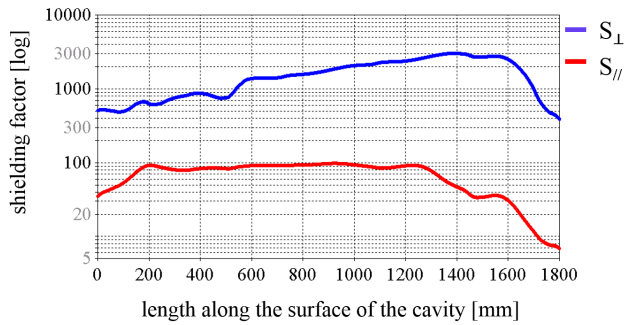

Figure 6: Rotationally averaged shielding factor along the surface of the cavity for both directions of the applied field. Individual results of the four cavities averaged.

By extending the length of the cold magnetic shield at the side of the tuner the penetrating field from this side can be reduced. An early design of a long united cold shield putting shielding covers around the tuner is shown in Figure 7. The simulation results of this structure (Fig. 8) show that although the penetrating field from the tuner side is reduced in comparison with a configuration of four cold shields without tuner covers the overall shielding efficiency is reduced. This happens because of the strong magnetic coupling between the cold shields through the tuner covers. For that reason the implementation of this design was abandoned.

Compensation Coils

In order to reduce the field penetrating from the tuner side and enhance the overall $S_\parallel$ the option of using four compensating coils has been investigated. The coils are

ISBN: 978-3-95450-191-5 doi:10.18429/JACoW-SRF2017-MOPB090

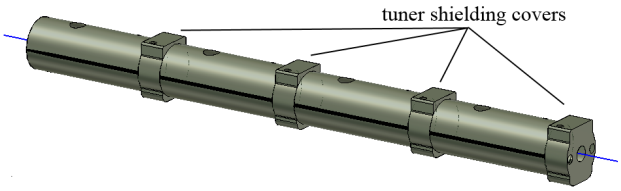

Figure 7: Design of a united cold shield with tuner shielding covers.

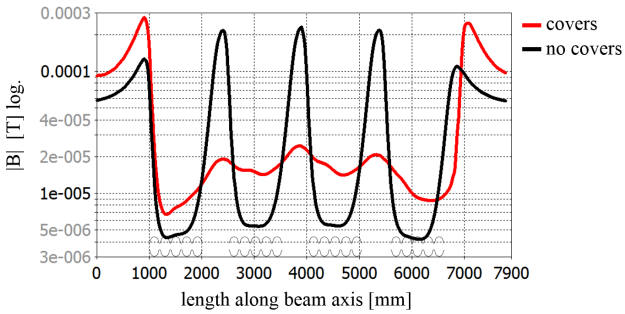

Figure 8: Absolute value of magnetic field on the beam axis. The position of the cavities is shown at the bottom of the plot. Applied field: $B_{\parallel}$ =50 µT

positioned outside of the vacuum vessel at the level of the four tuners (Fig. 9). By carefully optimizing the electric current values of the coils, the penetrating field is being compensated to a great extend as Figure 10 shows.

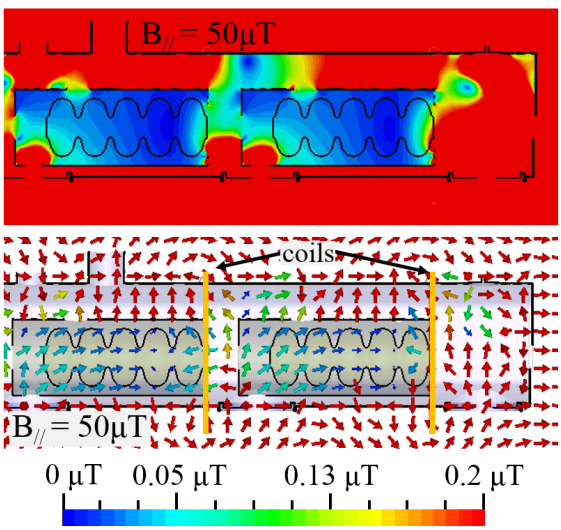

Figure 9: Simulation of cold and warm magnetic shields and of compensation coils. Absolute value of the magnetic field (up) and magnetic field vector (down) for the case of $B_{\parallel}$. Only half shield is presented.

An important point in the optimization of the coils is that by reducing the field on the tuner side of the cavity, the field on the next cavity is also being reduced. Since the compensating field reaching the next cavity is lower, the optimized solution suggests a stronger compensating field

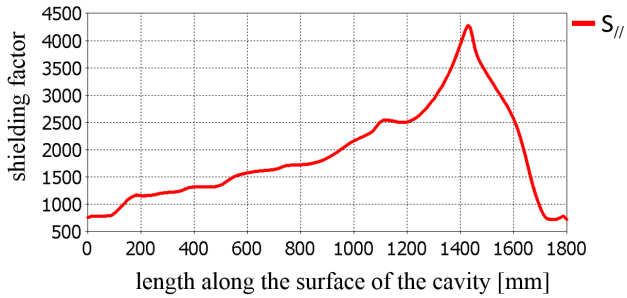

Figure 10: Rotationally averaged shielding factor along the surface of the cavity for $B_{\parallel}$. Individual results of the four cavities averaged.

in comparison with the one needed to compensate directly the field on the tuner side. This explains why the optimized $S_{\parallel}$ presents a peak that is not aligned with the coil position. This behaviour puts also a limit to the compensation that can be achieved. Nevertheless, as shown in Figure 10 the $S_{\parallel}$ has now increased to values much higher than 500. The electric current of the four coils varies from 60 – 65 amperes for each.

MAGNETIC FIELD CONDITIONS OF THE HG CRYOMODULE

In order to optimize the design of the magnetic shield it is important to investigate the magnetic conditions inside the cryomodule. For this purpose ambient magnetic field measurements have been realised in the interior volume and in the vicinity of the HG cryomodule which has been recently manufactured and delivered to CERN. The measurements are presented in Figure 11 and they show that the cryomodule contributes to the shielding with a shielding factor between 2.5 to 3. A small deterioration of the shielding factor is observed close to the middle of the vessel. On-spot measurements showed that the weld near the middle of the vessel (Fig. 12) is slightly magnetized without however raising any concerns for the magnetic shielding design.

If the vacuum vessel is slightly magnetized then part of the shielding that is observed might be due to compensation by the field induced by the vessel. In this case the shielding efficiency will be different for different orientations of the shield. For this reason, measurements have been done with a rotated shield by 180^o around y-axis to investigate the invariance of the shielding of the z-component to the relative position of the vessel in the ambient magnetic field. The results have shown that the shielding factor is the same for a rotated vessel thus the vessel is slightly magnetic but not magnetized.

CONCLUSION

The sub-µT magnetic shielding design for the HG test cryomodule has been presented. The shielding is achieved in three stages: the use of cold and warm shielding and of compensation coils. Magnetostatic simulation results reveal the

ISBN: 978-3-95450-191-5 doi:10.18429/JACoW-SRF2017-MOPB090

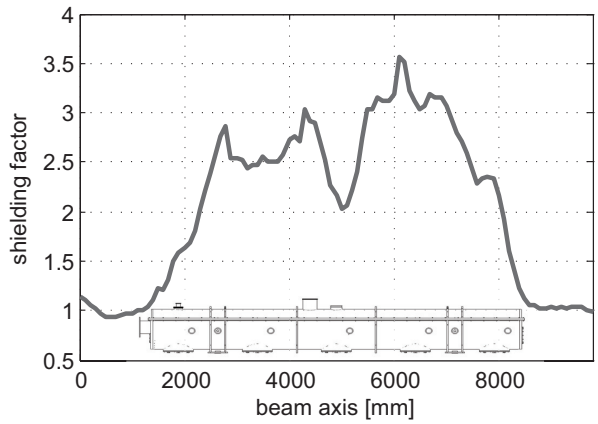

Figure 11: Shielding factor of the HG vacuum vessel measured along the beam axis. The position of the vessel is shown at the bottom of the plot.

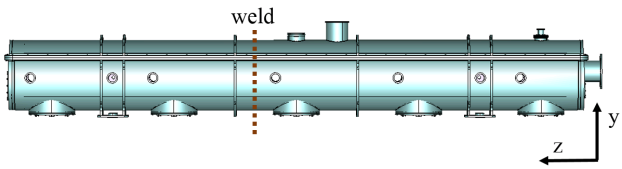

Figure 12: The High-Gradient cryomodule vacuum vessel.

efficiency and limits of every stage. Issues of consideration for an alternative cryomodule design have been addressed concerning the tuner side of the cold magnetic shield. The shielding factor for both $B_{\perp}$ and $B_{\parallel}$ reached values higher than 500. Finally, the magnetic shielding efficiency and magnetization of the HG cryomodule have been measured.

ACKNOWLEDGEMENTS

We would like to thank Juliette Plouin from CEA Saclay and Georgios Voulazeris from Magnetic Shields Limited UK for fruitful discussions and knowledge transfer.

REFERENCES

[1] J. Halbritter, *Zeitschrift fur Physik* 238 (1970) 466

[2] S. Aull and J. Knobloch, "Depinning of Trapped Magnetic Flux in Bulk Niobium SRF Cavities", https://arxiv.org/abs/1507.04105

[3] M. Checchin *et al.*, "Nature of Quality Factor Degradation in SRF Cavities due to Quench", in *Proc. SRF2015*, Whistler, BC, Canada, https://doi.org/10.18429/JACoW-SRF2015-MOBA05

[4] A. Mager, "Magnetic Shielding Efficiencies of Cylindrical Shells with Axis Parallel to the Field", *Journal of Applied Physics* 39, 1914 (1968), http://dx.doi.org/10.1063/1.1656455

[5] Takanori Okoshi, "Demagnetizing Factors of Rods and Tubes Computed from Analog Measurements", *Journal of Applied Physics* 36, 2382 (1965), http://aip.scitation.org/doi/10.1063/1.1714495

[6] M. Sato and Y. Ishii, "Simple and approximate expressions of demagnetizing factors of uniformly magnetized rectangular rod and cylinder", *Journal of Applied Physics* 36, 2382 (1965), http://aip.scitation.org/doi/abs/10.1063/1.343481

[7] R. I. Joseph, "Ballistic Demagnetizing Factor in Uniformly Magnetized Cylinders", *Journal of Applied Physics* 37, 4639 (1966), http://aip.scitation.org/doi/abs/10.1063/1.1708110

[8] Masuzawa *et al.*, "Magnetic Shielding: Our Experience with Various Shielding Materials", in *Proc. SRF2013*, Paris, France, paper WEIOD02.

[9] Juliette Plouin, "Magnetic shield design for the ESS medium and high beta cavities", ESS Technical. Report DN: ESS-0023089.

[10] Private communication with APERAM and Magnetic Shields Limited – UK.

[11] WMM 2015 – World Magnetic Model-United States' National Geospatial-Intelligence Agency (NGA) – United Kingdom's Defence Geographic Centre (DGC).